Combustion, Explosion, and Shock Waves, Vol. 43, No. 4, pp. 482–491, 2007

Analysis of Fractured Rock and Gas Flow Interaction in Explosion Simulations

S. Mohammadi[1] **and A. Bebamzadeh**[1]

UDC 539.379

Translated from *Fizika Goreniya i Vzryva*, Vol. 43, No. 4, pp. 127–137, July–August, 2007.
Original article submitted March 14, 2006.

In this study, an attempt has been made to adopt a combined finite discrete element methodology to couple gas dynamics equations and solid deformation states to develop a numerical tool for simulation of blast damage in brittle solid media such as rocks. A standard finite-element method is used, accompanied by strain softening behavior for modeling initiation and propagation of solid cracks due to high gas pressures. This variable high pressure is governed by the gas mass and momentum conservation equations. The gas behavior is fully coupled by the solid deformation which changes the density and porosity required in the gas dynamics equations and is based on new modifications to the recently proposed approach by the same authors. The proposed model for the flow of the detonation gas allows for evaluation of the spatial distribution of pressure and mass of the detonation gas over a complex geometry of cracked/fragmented solid (rock) model. Full geometric and material nonlinearities are taken into account by using a fully deformable finite-element mesh and cracked/fragmented discrete elements. Local adaptive remeshing (enrichment) techniques are used to geometrically simulate the crack propagation.

Key words: rock blasting, explosion, coupled gas–solid interaction, gas flow, finite/discrete element method.

INTRODUCTION

Explosion is frequently used in mining industry and tunneling engineering, where large rock masses are cracked and fragmented into small pieces by detonating a specific amount of an explosive material poured into boreholes. Several experiment-based empirical formulas have been proposed for estimating the initial borehole geometry and mechanical properties of the explosive material to achieve a specific post-blast outcome. The Kuz–Ram model for fragmentation is amongst the frequently used approaches, and several computer codes have been developed based on this method [1].

On the other hand, several attempts have been made over the years to develop numerical algorithms for a more realistic simulation of this highly complex phenomenon. Involvement of various mechanical behaviors in different fields, such as plasticity, fracture mechanics, gas dynamics, and chemical/mechanical behavior of detonation and explosion, however, has made the numerical modeling of an intact or fractured medium subjected to explosive loading as one of the most difficult engineering simulations.

A strong coupling exists between the gas and solid phases. Detonation causes a phase change of the explosive material into a gas with high pressure and temperature. Part of the amount of energy released by the explosive material is transmitted to the solid mass and causes subsequent deformation, acceleration, fracture, and fragmentation of the solid material. Gas expansion and its flow within the crack openings as well as the energy consumption for solid deformation reduce the gas pressure. Therefore, gas explosion and cracking are strongly coupled phenomena applying the gas pressure onto the solid body and causing its subsequent deformation and cracking, while changing gas characteristics, such as pressure and density [2].

[1]School of Civil Engineering, University of Tehran; smoham@ut.ac.ir.

0010-5082/07/4304-0482

Among several gas pressure-solid deformation models that have been proposed in recent years [1–5], the simplest model was based on a user-defined pressure-time curve [1], lacking any interaction phenomena and resulting in a user-dependent cracking solution. A simple but more exact detonation gas model was proposed by Munjiza [3], which was based on a no-gas-flow model within a combined finite/discrete element methodology. More recently, a new class of gas flow models have been developed, which somehow simulate the gas flow within the crack opening [4, 5]. They are classified into two main classes; the first class requires detecting the gas flow within independent cracks of complex geometry and involves rather difficult contact-detection algorithms, and the second class is designed to simulate an independent flow within a porous medium equivalent to a cracked solid medium. The main challenge of the second class of simulations is how to estimate a realistic porosity [6–10].

To facilitate the development of an efficient and reliable numerical approach for the analysis of explosion, a relatively complex interaction algorithm is proposed, which adopts two independent meshes for the analysis of solid and gas phases. The equations of the gas phase in the porous medium are used to compute pressure, mass transfer, energy, and expansion of the gas at each specified point [11]. The solution for the solid phase is found, based on the derived gas-pressure loading using a finite/discrete element (FE/DE) methodology [12–14], which is capable of analyzing the interaction among a wide range of discrete bodies/materials. It is necessary to couple the FE/DE method with the gas dynamics equations to analyze the dynamic behavior of fracturing rock masses in blasting. When the gas–solid interaction model is implemented into the combined FE/DE method, the model will be able to evaluate the spatial distribution of the pressure of the detonation gas, the work done by the expanding gas, and the total mass of the detonation gas as functions of time, indicating the ability of the model to respond to changes in both the mass of the explosive charge and the size of the solid block being fractured [15].

The proposed algorithm allows for corporation of new lines/edges/bodies created from fracturing and fragmentation of the original model. A bilinear Rankine strain softening plasticity model is employed to account for the fracture energy release during the creation/propagation of cracks [12].

The present paper provides basics of a novel numerical approach for simulation of the highly complex problem of rock blasting. The proposed methodology is taking only the opening steps to illustrate how such an engineering problem comprising highly complex thermo-mechanical phenomena can be efficiently discretized into better developed modules and then combined to accomplish feasible results. Subject to further investigations, the method is expected to be bale to provide some numerical-based guidelines for simulation of explosive loadings and gas–solid interaction problems and to introduce a reliable tool for the analysis of complex phenomena of rock blasting. In order to achieve this long-range goal, however, further studies are required.

Despite the fact that real blasting situations are three-dimensional problems, however, in this paper only 2D models are presented. The present 2D approach is extremely complex, and it is only by proper development, verification, and calibration that a move to general 3D applications is feasible.

GAS AND SOLID PHASES

Microscopic and macroscopic equations of state have already been developed to study different physical behavior of the gas and solid phases of a porous medium [15]. Each phase may be considered separately or studied within a multiphase porous medium. Here, only the necessary two-dimensional equations of conservation of mass and momentum are examined. Similar equations can be derived and implemented for three-dimensional multiphase problems.

The microscopic mass-balance equation for the solid or gas phases can be defined as [11]:

$$\frac{\partial \rho}{\partial t} + \operatorname{div}(\rho \dot{r}) = 0, \tag{1}$$

where $\dot{r}$ is the velocity of the phase at a fixed point in space and ρ is the volume-averaged mass density. On a macroscopic level, the mass-balance equation of the gas phase can be written as

$$\frac{\partial}{\partial t}\left(n\rho^g\right) + \operatorname{div}(n\rho^g \boldsymbol{v}^g) = 0, \tag{2}$$

where ρ^g is the gas-phase averaged density, $\boldsymbol{v}^g$ is the mass-averaged gas velocity, and n is the volume fraction. The macroscopic linear momentum takes the form [11]

$$n\boldsymbol{v}^{gs} = \frac{\boldsymbol{k}k^{rg}}{\mu^g}\left[-\nabla p^g + \rho^g(\boldsymbol{g} - a^s - a^{gs})\right], \tag{3}$$

where μ^g is the dynamic viscosity, p^g is the pressure in the gas, $\boldsymbol{g}$ is the gravitational acceleration, a^{gs} is the relative acceleration, $\boldsymbol{k}$ is the permeability tensor of the medium, and k^{rg} is the relative permeability parameter. By assuming the solid-phase velocity to be zero ($\boldsymbol{v}^s = 0$), $\mu^g = 1$, and neglecting the gravitational acceleration and the relative and solid-phase accelerations in comparison to very high pressures, Eq. (3) reduces to

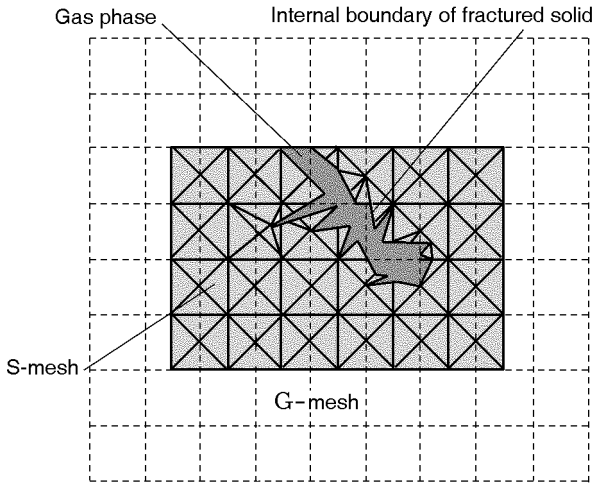

Fig. 1. Two-mesh model for coupling the solid and gas phases.

$$n\boldsymbol{v}^g = \boldsymbol{k}k^{rg}(-\nabla p^g). \tag{4}$$

The mass-momentum equation is formed by combining Eqs. (2) and (4):

$$\frac{\partial}{\partial t}(n\rho^g) + \operatorname{div}\left[\boldsymbol{k}k^{rg}\rho^g(-\nabla p^g)\right] = 0. \tag{5}$$

COUPLED GAS FLOW-SOLID INTERACTION

In this section, an interaction algorithm based on a two-mesh model is introduced. Two-mesh models have been previously proposed for solving coupled problems. Munjiza [3] discussed potential steps for solving a gas–solid interaction problem but failed to develop and implement the formulation and instead only used a simple no-gas-flow model to solve several blasting problems. Mohammadi et al. [15] recently developed a new two-mesh model by taking into account the gas flow within the fractured/deformed solid surroundings. Here the same methodology is followed, with new modifications to improve the shortcomings of the original approach.

The present algorithm uses one mesh for modeling the solid material (S-mesh), and the second mesh is used for modeling the gas phase (G-mesh), as depicted in Fig. 1. Standard procedures are adopted to map all the necessary data and state variables from the solid mesh into the gas mesh and vise versa. Mapped data onto the G-mesh may be used for evaluation of gas porosity, while the gas mapped data onto the S-mesh are primarily used to apply the resulting updated pressure on finite elements and/or nodes. The procedure is continuously updated in successive time steps.

The principles of mechanics of porous media are adopted to analyze the G-mesh. First, it is assumed that no solid exists in the gas phase, and only the equations of mass and momentum are satisfied. The solid phase contributes to the equilibrium equations only through the permeability coefficient $\boldsymbol{k}$. Equation (5) for the gas phase ($n = 1$) takes the form

$$\frac{\partial}{\partial t}(\rho^g) + \operatorname{div}\left[\boldsymbol{k}k^{rg}\rho^g(-\nabla p^g)\right] = 0 \tag{6}$$

subject to the following boundary conditions:

$$\rho^g\boldsymbol{k}k^{rg}(-\nabla p^g)^T \cdot \boldsymbol{n} = 0 \quad \text{on boundary } \Gamma_g^q \tag{7}$$

($\boldsymbol{n} = \{\boldsymbol{n}_x, \boldsymbol{n}_y, \boldsymbol{n}_z\}^T$ is the normal vector; no input mass flow is considered).

The weighted residual form of Eqs. (6) and (7) can be written as [15]

$$\int_\Omega \boldsymbol{W}^T\left\{\nabla^T\left[\boldsymbol{k}(-\nabla p^g)\right] + \frac{\partial \rho^g}{\partial t}\right\} d\Omega + \int_{\Gamma_g^q} \boldsymbol{W}^T\left[\boldsymbol{k}(-\nabla p^g)^T \cdot \boldsymbol{n}\right] d\Gamma = 0, \tag{8}$$

where $\boldsymbol{W}$ is a weighted residual function. Applying the Green theorem, we obtain

$$\int_\Omega (\nabla \boldsymbol{W})^T\boldsymbol{k}\rho^g\nabla p^g d\Omega + \int_\Omega \boldsymbol{W}^T\frac{\partial \rho^g}{\partial t}\, d\Omega = 0. \tag{9}$$

The pressure p^g can be defined based on the nodal pressures $\bar{p}^g$ using the standard finite-element shape functions $\boldsymbol{N}_p$:

$$p^g = \boldsymbol{N}_p\bar{p}^g. \tag{10}$$

In a Galerkin formulation, the weighted residual functions can be assumed to be the same as the shape functions, $\boldsymbol{N}_p = \boldsymbol{W}$; therefore, Eq. (9) reduces to

$$\int_{d\Omega} (\nabla \boldsymbol{N}_p)^T\boldsymbol{k}\rho^g\nabla \boldsymbol{N}_p\bar{p}^g d\Omega + \frac{1}{\partial t}\int_\Omega \boldsymbol{N}_p^T\partial\rho^g d\Omega = 0. \tag{11}$$

Equation (11) can be interpreted as representing the change in mass per unit time, and it can be rewritten in a more appropriate form

$$\boldsymbol{M}_{t+\Delta t} = \boldsymbol{M}_t - \Delta t\boldsymbol{H}_t^p\bar{p}_t^g, \tag{12}$$

where $\boldsymbol{H}_t^p$ is the permeability matrix defined by

$$\boldsymbol{H}_t^p = \int_\Omega (\nabla \boldsymbol{N}_p)^T\boldsymbol{k}\rho^g\nabla \boldsymbol{N}_p d\Omega. \tag{13}$$

The simplest possible option for the G-mesh, which is a square-cell structured grid, is adopted. The shape function $\boldsymbol{N}_p$ and its derivative can then be defined as

$$\boldsymbol{N}_p = 0.25 \times [(1-x)(1-y)\,(1+x)(1-y)\,(1+x)(1+y)\,(1+x)(1+y)], \tag{14}$$

$$\nabla \boldsymbol{N}_p = 0.25 \times \begin{bmatrix} -(1-y) & (1-y) & -(1+y) & (1+y) \\ -(1-x) & -(1+x) & (1-x) & (1+x) \end{bmatrix}, \tag{15}$$

and $d\Omega = a^2 dx\, dy$, where a is the size of the square element.

If the simplest approximation of assuming mean values of $\bar{\rho}^g$ and $\bar{K}$ over the gas element volume is considered, a simple matrix can then be computed:

$$\boldsymbol{H}_t^p = \frac{1}{6}\, a^2 \bar{\rho}^g \bar{K} \begin{bmatrix} 4 & -1 & -1 & -2 \\ -1 & 4 & -2 & -1 \\ -1 & -2 & 4 & -1 \\ -2 & -1 & -1 & 4 \end{bmatrix}. \tag{16}$$

A more accurate solution is achieved if similar shape functions are used to approximate the variations of density and porosity within the element. After lengthy manipulations, one can derive the components of the symmetric $\boldsymbol{H}_t^p$ matrix

$$\boldsymbol{H}_{ij}^p = \frac{1}{360} \boldsymbol{K}^T \boldsymbol{D}_{ij} \rho, \tag{17}$$

where

$$\boldsymbol{K}^T = [K_1\ K_2\ K_3\ K_4], \tag{18}$$

$$\boldsymbol{\rho}^T = [\rho_1\ \rho_2\ \rho_3\ \rho_4], \tag{19}$$

and D_{ij} are the components of the symmetric D matrix:

$$D_{11} = \begin{bmatrix} 48 & 18 & 18 & 6 \\ 18 & 28 & 6 & 8 \\ 18 & 6 & 28 & 8 \\ 6 & 8 & 8 & 8 \end{bmatrix},$$

$$D_{12} = \begin{bmatrix} -18 & -8 & -3 & -1 \\ -8 & -18 & -1 & -3 \\ -3 & -1 & 2 & 2 \\ -1 & -3 & 2 & 2 \end{bmatrix},$$

$$D_{13} = \begin{bmatrix} -18 & -3 & -8 & -1 \\ -3 & -14 & -1 & -2 \\ -8 & -1 & -18 & -3 \\ -1 & -2 & -3 & -2 \end{bmatrix},$$

$$D_{14} = \begin{bmatrix} -12 & -7 & -7 & -4 \\ -7 & -12 & -4 & -7 \\ -7 & -4 & -12 & -7 \\ -4 & -7 & -7 & -12 \end{bmatrix},$$

$$D_{22} = \begin{bmatrix} 28 & 18 & 8 & 6 \\ 18 & 48 & 6 & 18 \\ 8 & 6 & 8 & 8 \\ 6 & 18 & 8 & 28 \end{bmatrix},$$

$$D_{23} = \begin{bmatrix} -12 & -7 & -7 & -4 \\ -7 & -12 & -4 & -7 \\ -7 & -4 & -12 & -7 \\ -4 & -7 & -7 & -12 \end{bmatrix},$$

$$D_{24} = \begin{bmatrix} -18 & -3 & -8 & -1 \\ -3 & 2 & -1 & 2 \\ -8 & -1 & -18 & -3 \\ -1 & 2 & -3 & 2 \end{bmatrix},$$

$$D_{33} = \begin{bmatrix} 28 & 8 & 18 & 6 \\ 8 & 8 & 6 & 8 \\ 18 & 6 & 48 & 18 \\ 6 & 8 & 18 & 28 \end{bmatrix},$$

$$D_{34} = \begin{bmatrix} 2 & 2 & -3 & -1 \\ 2 & 2 & -1 & -3 \\ -3 & -1 & -18 & -8 \\ -1 & -3 & -8 & -3 \end{bmatrix},$$

$$D_{44} = \begin{bmatrix} 8 & 8 & 8 & 6 \\ 8 & 28 & 6 & 18 \\ 8 & 6 & 28 & 18 \\ 6 & 18 & 18 & 48 \end{bmatrix}. \tag{20}$$

The solution procedure can now be summarized into the following steps:

1. Define the initial solid mesh (S-mesh) and gas grid (G-mesh). A general finite-element unstructured mesh generator can be used to create an appropriate mesh, refined around the explosion borehole. A structured square-element G-mesh is used.

2. Setting the initial values of $\boldsymbol{M}_n^0$ and p_n^0 for the G-mesh nodes, followed by the evaluation of the solid volume associated to each node of the G-mesh. The solid volume is then updated at a pressure p according to the equation of state (EOS) for the solid material, allowing for an accurate estimation of the porosity volume of the G-mesh nodes.

3. By computing the initial mean density $\bar{\rho}$ and the initial permeability of the element K_0, the permeability matrix H_{pe}^0 is calculated.

4. New nodal pressures can be determined by a simple iterative procedure involving an initial assumption for the pressure, calculating its associated work due to a change in porosity, and predicting the new pressure from the non-perfect gas pressure law until an allowable tolerance is reached.

5. After a converged solution is found for the pressure, the S-mesh nodal pressures are interpolated from the G-mesh nodal values. The solid model is then analyzed using an explicit dynamic FE/DE method, including a crack analysis based on the material model for the solid, and necessary re-meshing and geometric crack modeling.

6. Again, new values for porosity in the G-mesh are computed, and new values for the mass are computed from the nodal pressures p_n: $\boldsymbol{M}_n^1 = \boldsymbol{M}_n^0 - \Delta t \boldsymbol{H}_{pe}^0 \bar{p}_n^0$.

NUMERICAL VERIFICATION

In this section, three numerical simulations are presented to assess the performance of the method. The main attention is focused on problems unlikely to be examined by other available numerical tools, because of the complexity of the problem and interactions among various contributing phenomena.

For the sake of simplicity in preparing the initial geometric data, original models are assumed to be intact continuous solid rocks. The solid phase may then be cracked and fragmented when subjected to high blast pressures. This clearly shows the capability of the approach in dealing with discontinuities, such as discontinuous rock media subject to explosive loadings, planned for future studies. Structured square-element G-meshes are used for all numerical simulations.

Example 1. The first example is to simulate the behavior of a solid chamber filled with the explosive material when subjected to explosion. This problem has been used in a number of previous works [3, 13, 15] to verify various gas–solid interaction formulations.

Figure 2 illustrates the initial geometry of the chamber and defines the basic information required for the explosive material (mass 148 kg, density 240 kg/m^3, and detonation velocity 1725 m/sec). In this test, any change in gas pressure is caused by the escaping gas from the open end of the chamber.

Figure 3 compares the pressure history at the left end of the chamber, obtained by the present approach, to the results reported in [3] and experimentally measured pressure history. This close agreement is an indication of how the proposed model can be efficiently used to simulate the variations of pressure due to the escaping gas from the explosive holes, as well as potential cracks or openings.

Exactly similar results were reported by an algorithm earlier developed by the authors [15], showing that the gas flow simulations resulting from a changing gas volume by both approaches are the same and very close to other available results.

Example 2. An example previously studied by Munjiza [3] is simulated. A 13 m long borehole close to an edge of a rock mass is considered. Only nine meters from the bottom of the borehole are filled with an explosive material, leaving the top part of the borehole empty. Figure 4 illustrates the problem geometry and the finite-element model. The following mechanical properties of the rock are assumed: modulus of

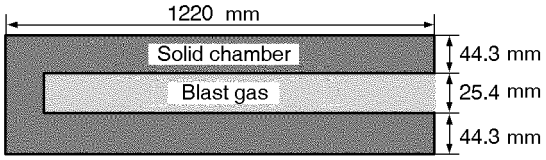

Fig. 2. Geometry of the solid container and properties of the explosive material: mass 148 kg, density 240 kg/m^3, and detonation velocity 1725 m/sec.

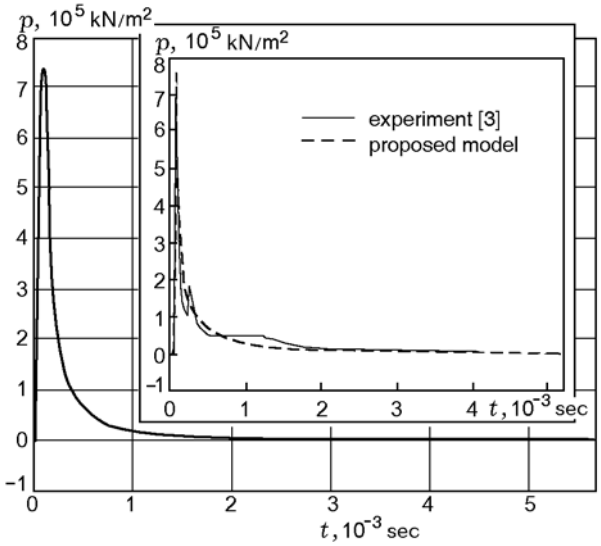

Fig. 3. Pressure histories of the proposed approach, Munjiza [3], and the experimental results.

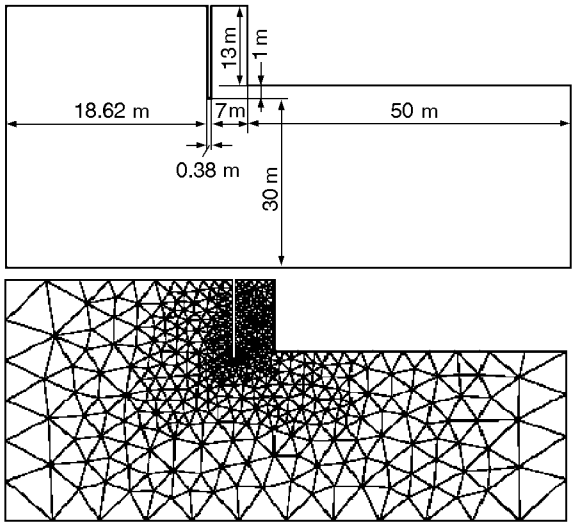

Fig. 4. Geometric definition and finite-element modeling of rock blasting with a single explosive borehole.

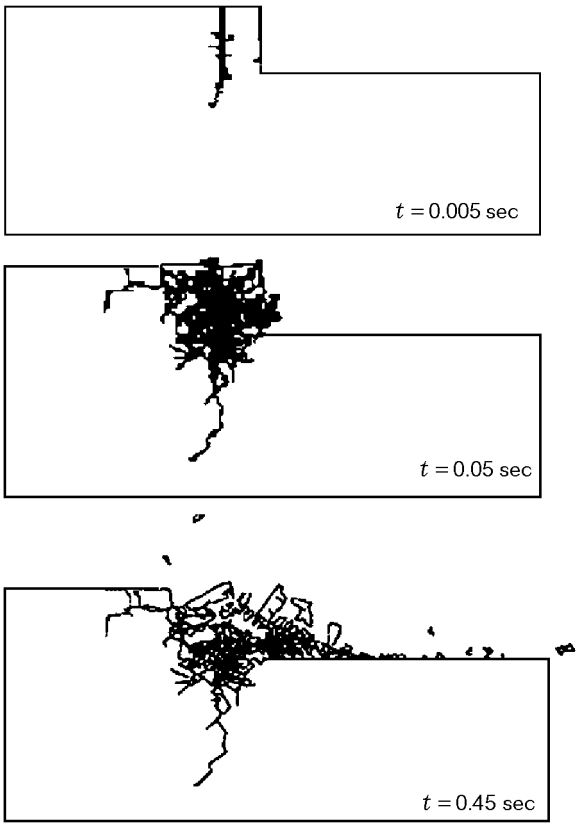

Fig. 5. Crack propagation and fragmentation patterns at successive time steps.

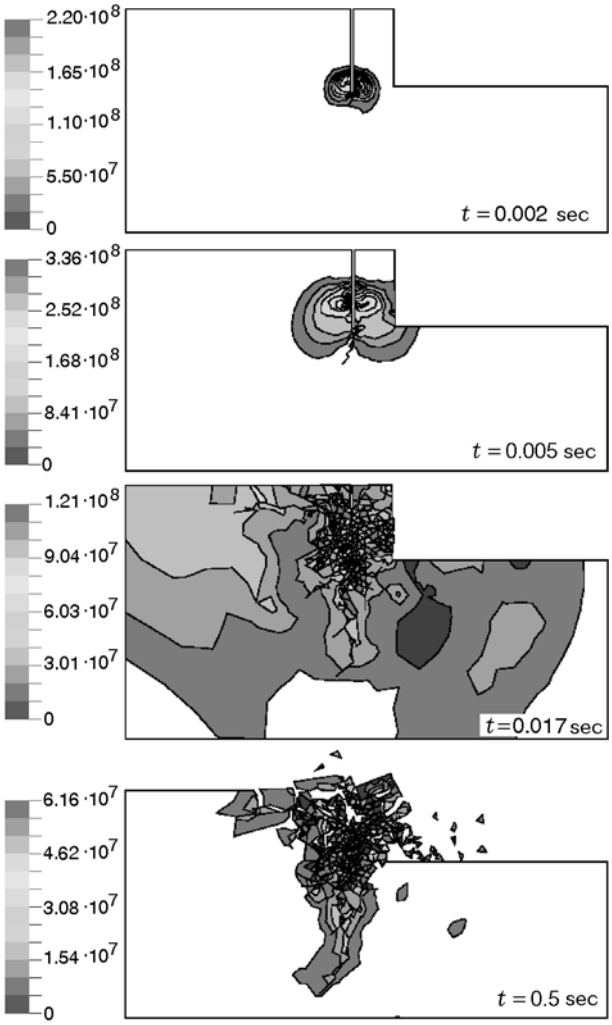

Fig. 6. Effective stress contours at different times.

elasticity $E = 28{,}000$ MPa, Poisson's ratio $\nu = 0.1$, density $\rho = 4200$ kg/m^3, rate of volume reduction $\lambda = 1.2 \cdot 10^{10}$ kg/m^3, fracture energy release rate $G_f = 250$ N$\cdot$m/m^2, tensile strength $\sigma_t = 50$ MPa, and compressive strength $\sigma_{\text{comp}} = 2500$ MPa. The properties of the explosive material are as follows: initial density $\rho_0 = 276.165$ kg/m^3, density at an initial point f $\rho_f = 850$ kg/m^3, parameter $\alpha = 10.99 \cdot 10^{-10}$, imperfect gas constant $\gamma = 2.5$, pressure at the point f $p_f = 3.4 \cdot 10^8$ N/m^2, time of ignition $t_G = 10^{-9}$ sec, blast specific energy $Q_e = 3700$ kJ/kg, velocity of detonation $D = 1725$ m/sec, volume of the borehole associated with the charge 0.3429, and permeability coefficient $\boldsymbol{k} = 3 \cdot 10^{-8}$ m^2/(Pa$\cdot$sec).

An adaptive unstructured triangular finite-element mesh is generated to create a very fine mesh of finite elements around the borehole and where stress concentration and cracking are expected to occur, while coarser finite elements are used to reduce the computational costs and computer time (see Fig. 4). In total, 876 finite elements are used at the beginning of the analysis.

All boundaries, except for the top free edges are assumed to be constrained in both x and y directions. It is assumed that these boundary edges are far enough from the borehole and do not affect the solution by reflecting the generated waves. Therefore, no special non-reflecting or absorbing boundary conditions are required. It is important to note that such boundary conditions are mandatory for a realistic analysis of explosion in order to simulate an infinite domain by a finite model.

Figure 5 shows the progressive cracking phenomena at successive time steps. By detonating the explosive material, high gas pressures are generated and then applied to the solid material, causing rock cracks around the borehole. By increasing the blast gas pressure, the solid rock is further cracked and fragmented.

Figure 6 illustrates the development of effective stress bubble contours. It is initially generated symmet-

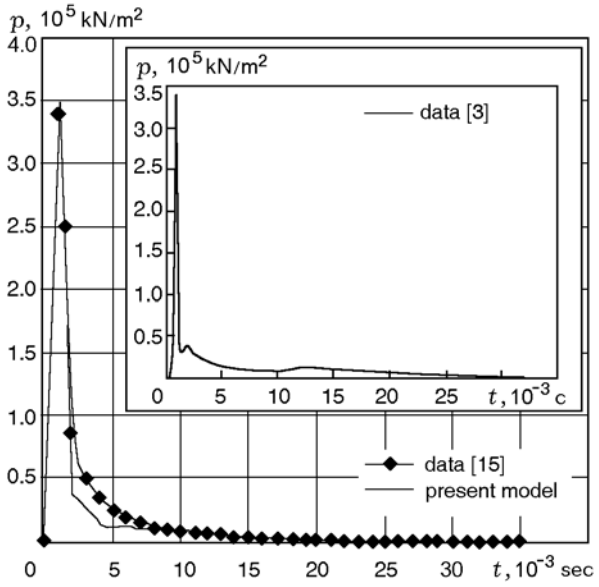

Fig. 7. Comparison of the predicted pressure history with the results obtained by the earlier developed algorithm [15] and in [3].

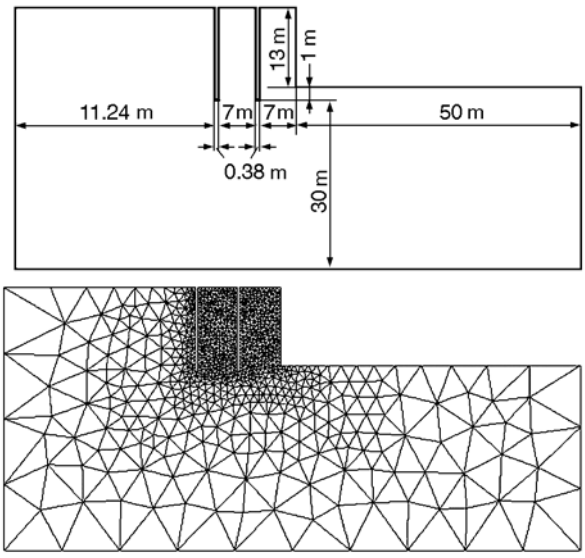

Fig. 8. Geometry and finite-element model for the two-borehole problem.

rically around the borehole base. After the rock cracking, however, the pressure distribution and the generated effective stress contours mainly follow the cracked geometry at any time.

Finally, Fig. 7 compares the gas pressure history at the bottom of the borehole predicted by the present approach with the one reported by Munjiza [3], where a simplified no-gas-flow algorithm was used.

Estimation of the fragment size distribution, throw or muck-pile form, and back-break geometry are of practical importance. Although qualitative estimations can be directly derived from the results depicted in Fig. 5, they may not be directly related to those practical engineering measures. In fact, it has not been a primary goal of this research at this stage to engage with calculation of such practical measures.

Example 3. The same rock mass defined in the previous example is reconsidered to simulate explosions at two boreholes, as depicted in Fig. 8, which also shows the finite-element mesh with over 2000 finite elements adaptively generated to create a fine distribution of elements around the boreholes while creating only a coarse mesh of elements elsewhere to keep the total size of the numerical model as minimum as possible.

First, non-simultaneous explosions are considered. The left borehole is detonated at the beginning of the analysis, followed by the explosion of the second borehole at 0.006 sec afterwards.

Figure 9 depicts the general patterns of effective stress contours at successive time steps from the initial borehole explosion until the early post stages of the second explosion. Development of the stress bubble is contained only around the right borehole, gradually extending toward the intact left hole. Immediately after the initiation of explosion at the second borehole, complex effective stress contours are predicted due to a very complex character of two explosive loadings and a complicated pattern of solid cracking and fragmentation.

Figure 9 also illustrates cracking and fragmentation patterns at successive time steps. It is clearly seen that extensive cracking/fragmentation is created around the first exploded borehole, while the solid material around the undetonated explosive hole remains almost intact at the very early stages of the simulation. Later, the cracking pattern reaches the boundaries of the second hole assumed initially as an empty hole for the solid phase. In fact, any overpressure or major deformation affecting the initial configuration or behavior of the second borehole prior to its detonation is neglected. The second explosion happens when the solid has already undergone extensive damage from the first explosive loading. It results in new cracking and fragmentation well beyond the original extent caused by the first explosion.

Simultaneous initiation of two blast holes directly behind each other is almost never used in practice; nevertheless, to compare the present algorithm with available results from other researchers and to study the effect of finite-element refinement on the final extent of the damaged material, the model is subjected to simultaneous explosions at two boreholes.

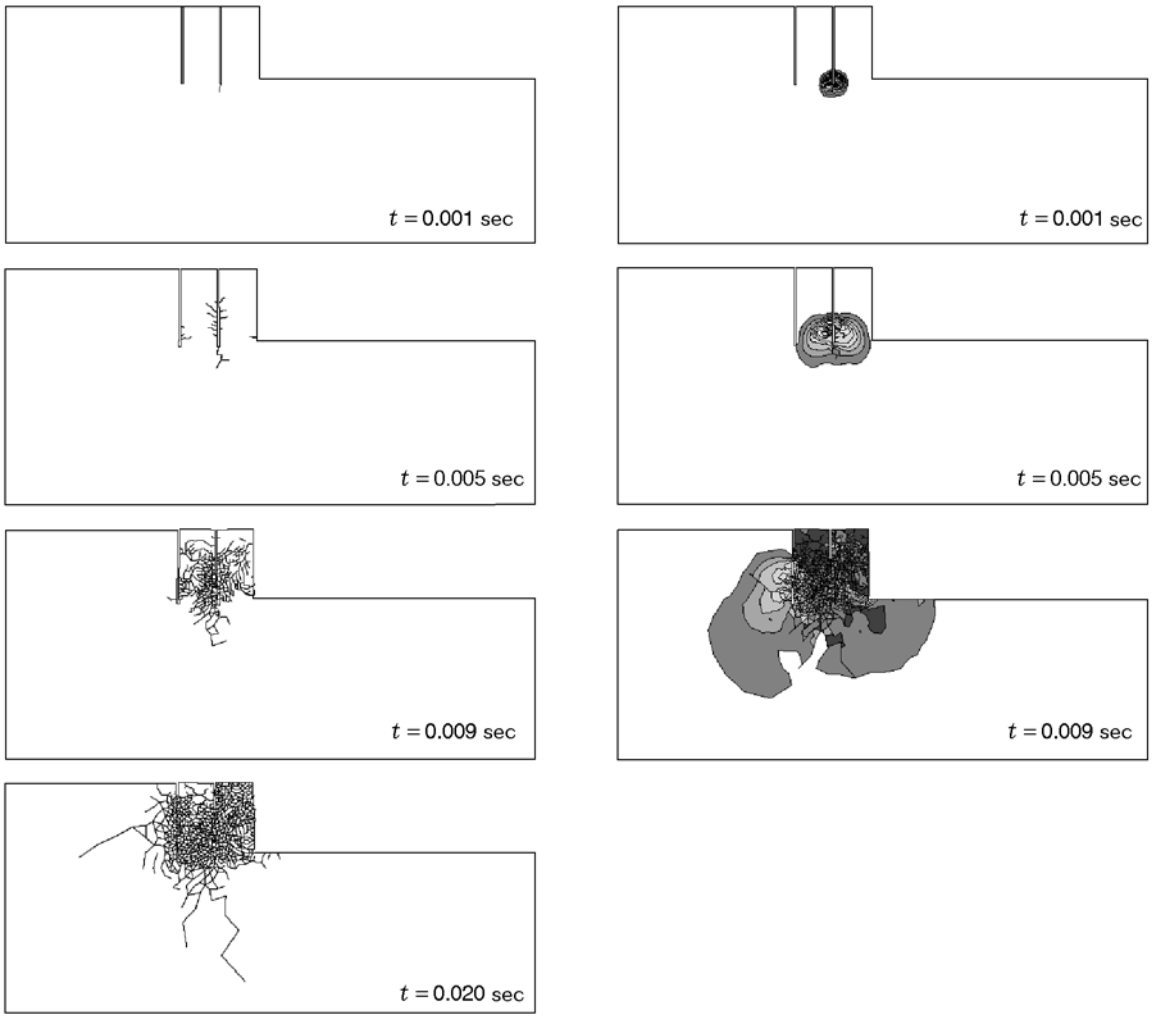

Fig. 9. Crack and fragmentation patterns (left) and development of effective stress bubble contours (right) at different time steps for non-simultaneous explosions.

Coarse and fine finite-element meshes were used to simulate the model and to compare the results for various finite-element models. The coarse mesh consists of 1000 nodes and 1000 elements, while 2000 nodes and 2100 elements create the fine mesh. In both cases, adaptive mesh generators have been used to create a very fine mesh around the boreholes while generating a coarse mesh elsewhere to keep the total size of the problem as minimum as possible. Similar boundary conditions as those in the previous example are applied for both meshes.

Figure 10 compares the cracking patterns at successive time steps for the coarse and fine meshes. They predict more realistic results than the previously reported rough results by Munjiza [3] (see Fig. 10b).

Conclusions. In this paper, a two-mesh coupled gas dynamics/solid mechanics interaction model is developed and implemented into a combined finite/discrete element methodology to simulate the complex behavior of rock blasting, which involves extensive fracture and fragmentation within the domain, affecting the pressure and density of the blast-induced gas. Several numerical simulations have been used to assess the performance of the proposed algorithm. They include theoretical benchmarks and simulations previously performed by other researches. The method, however, becomes numerically expensive as the size of the regular G-mesh is reduced to enhance the accuracy of the gas-related computations. Therefore, it is proposed to use a carefully designed independent adaptive G-mesh or a mesh similar to the S-mesh for future studies. Also, the effects of existing rock cracks or joints on the overall and local gas–solid interaction behavior can be studied. The present work is still far from a situation where

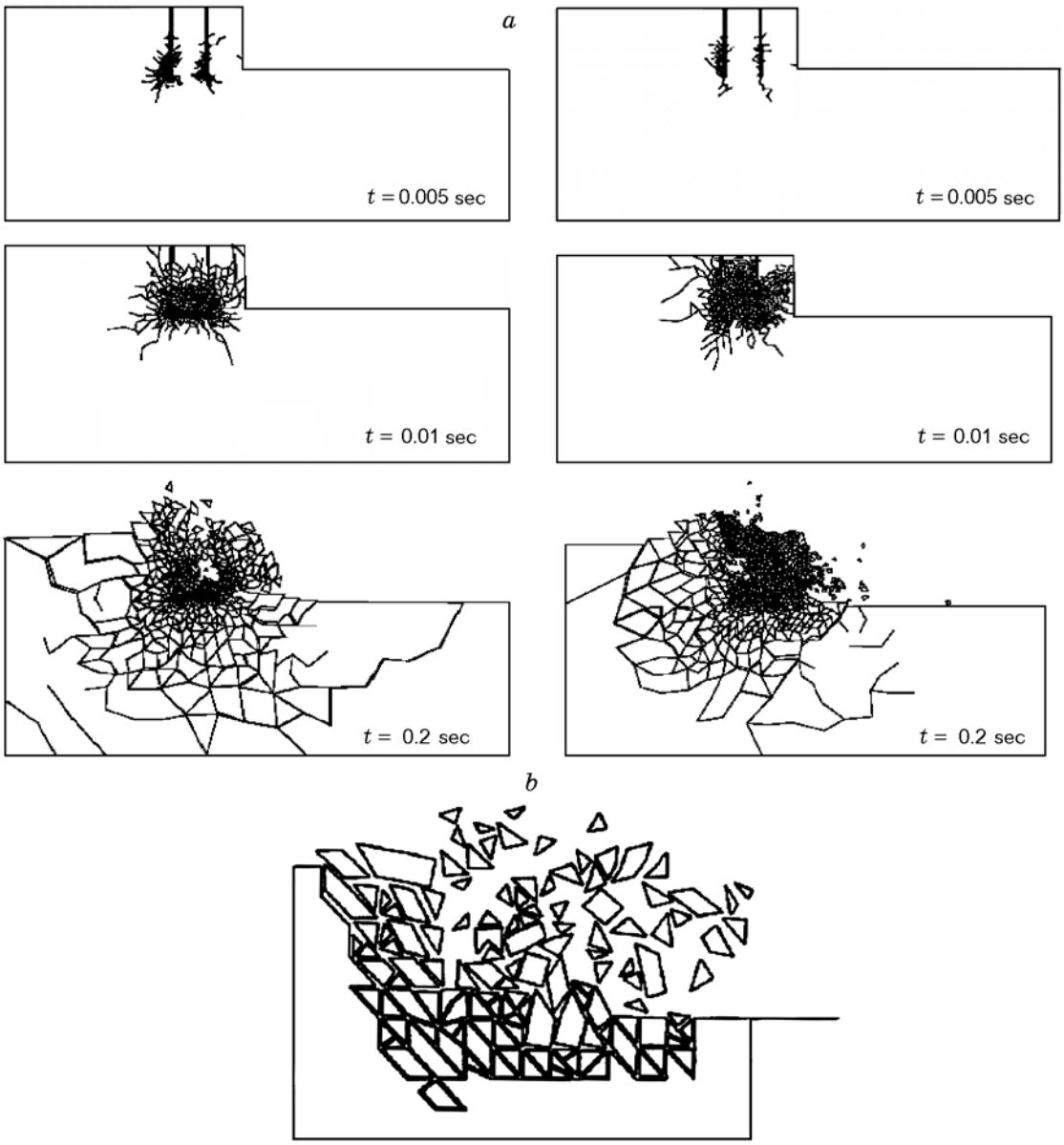

Fig. 10. Cracking and fragmentation patterns (a) at different time steps based on a simulation by a coarse mesh (left) and a fine mesh (right) for simultaneous explosions in comparison to the results by Munjiza [3] (b).

the results could be of practical use in rock engineering; however, it is a promising framework for future deterministic analysis of rock blasting by a well-developed finite-element software with direct practical interest and use.

REFERENCES

1. A. A. Bauer and D. Fratzos, "Finite element modeling of pre-split blasting using measured time curves," in: *Society of Explosive Engineers Annual Meeting*, Miami (1987).
2. L. Xian, N. Bicanic, D. R. J. Owen, and A. Munjiza, "Rock blasting simulation by rigid body dynamic analysis and rigid brittle fracturing model," in: *Proc. Int. Conf. on Nonlinear Engineering Computations*, Pineridge Press (1991), pp. 477–587.
3. A. Munjiza, "Discrete elements in transient dynamics of fractured media," Ph. D. Thesis, University of Wales Swansea (1992).
4. D. S. Preece, S. L. Burchell, and D. S. Scovira, "Coupled gas flow and rock motion modeling with comparison to bench blast field data," in: *Proc. 4th Int. Symp. on Rock Fragmentation by Blasting*, Vienna (1993), pp. 239–247.

5. A. Munjiza, J. P. Latham, and K. F. Andrews, "Detonation gas model for combined finite-discrete element simulation of fracture and fragmentation," *Int. J. Numer. Meth. Eng.*, **49**, 1495–1520 (2000).
6. R. H. Nilson, "An integral method for predicting hydraulic fracture propagation driven by gases or liquids," *Int. J. Rock Mech.*, **22**, 3–19 (1996).
7. D. S. Preece and B. J. Thorne, "A study of detonation timing and fragmentation using 3D finite element techniques and damage constitutive model," in: *Proc. 5th Int. Symp. of Rock Fragmentation by Blasting* (1996), pp. 147–156.
8. A. Daehnke, H. Rossmanith, and J. F. Schatz, "On dynamic gas pressure induced fracturing," *Int. J. Blasting Fragmentation*, **1**, 59–73 (1997).
9. R. E. Danell, T. Lewnardowski, and V. K. Laun Mai, "Influence of discontinuities on pre-splitting effectiveness," *ibid.*, pp. 27–41.
10. A. Minchinton and P. Lynch, "Fragmentation and heave modeling using coupled discrete element gas flow code," *ibid.*, pp. 49–59.
11. R. W. Lewis and B. A. Schrefeler, *The Finite Element Method in the Static and Dynamic Deformation and Consolidation of Porous Media*, Wiley (1998).
12. S. Mohammadi, *Discontinuum Mechanics Using Finite and Discrete Elements*, WIT Press (2003).
13. A. Munjiza, D. R. J. Owen, and N. Bicanic, "A combined finite-discrete element method in transient dynamics of fracturing solids," *Int. J. Eng. Comput.*, **12**, 145–174 (1995).
14. A. Munjiza, K. R. F. Andrews, and J. K. White, "Combined single and smeared crack model in combined finite-discrete element method," *Int. J. Numer. Methods Eng.*, **44**, 41–57 (1998).
15. S. Mohammadi and A. Bebamzadeh, "A coupled gas-solid interaction model for FE/DE simulation of explosion," *Finite Elem. Anal. Des.*, **41**, 1289–1308 (2005).